Editors' Suggestion Featured in Physics

Colossal Elastocaloric Effect in Ferroelastic Ni-Mn-Ti Alloys

Daoyong Cong,[1,*] Wenxin Xiong,[1] Antoni Planes,[2] Yang Ren,[3] Lluís Mañosa,[2] Peiyu Cao,[1] Zhihua Nie,[4] Xiaoming Sun,[1] Zhi Yang,[1] Xiufeng Hong,[1] and Yandong Wang[1]

[1]*Beijing Advanced Innovation Center for Materials Genome Engineering, State Key Laboratory for Advanced Metals and Materials, University of Science and Technology Beijing, Beijing 100083, China*

[2]*Departament de Física de la Matèria Condensada, Facultat de Física, Universitat de Barcelona, Martí i Franquès 1, E-08028 Barcelona, Catalonia, Spain*

[3]*X-ray Science Division, Argonne National Laboratory, Argonne, Illinois 60439, USA*

[4]*School of Materials Science and Engineering, Beijing Institute of Technology, Beijing 100081, China*

(Received 10 January 2019; published 26 June 2019)

Energy-efficient and environment-friendly elastocaloric refrigeration, which is a promising replacement of the conventional vapor-compression refrigeration, requires extraordinary elastocaloric properties. Hitherto the largest elastocaloric effect is obtained in small-size films and wires of the prototype NiTi system. Here, we report a colossal elastocaloric effect, well exceeding that of NiTi alloys, in a class of bulk polycrystalline NiMn-based materials designed with the criterion of simultaneously having large volume change across phase transition and good mechanical properties. The reversible adiabatic temperature change reaches a strikingly high value of 31.5 K and the isothermal entropy change is as large as 45 $\mathrm{J\,kg^{-1}\,K^{-1}}$. The achievement of such a colossal elastocaloric effect in bulk polycrystalline materials should push a significant step forward towards large-scale elastocaloric refrigeration applications. Moreover, our design strategy may inspire the discovery of giant caloric effects in a broad range of ferroelastic materials.

DOI: 10.1103/PhysRevLett.122.255703

Refrigeration has become an indispensable technology in our modern society, which is required in numerous application areas such as food preservation, cold-chain transportation, and air conditioning. Present refrigeration technologies are based primarily on vapor compression using environmentally harmful fluids which produce greenhouse gases and therefore raise serious environmental concerns [1–3]. It is imperative to develop alternative cooling technologies that are clean and highly efficient. Solid-state refrigeration based on magnetocaloric, electrocaloric, and elastocaloric effects (which refer to the adiabatic temperature change or the isothermal entropy change of the material upon the application of magnetic field, electric field, and stress, respectively) [4–8] is nowadays under extensive investigation worldwide. The magnetocaloric (electrocaloric) effect requires large magnetic (electric) fields [4,9] which can be costly and challenging to generate. Recently, elastocaloric refrigeration employing the large latent heat associated with stress-induced martensitic phase transition [10,11] has been identified by the U.S. Department of Energy as one of the most promising non-vapor-compression cooling technologies [1].

Implementation of elastocaloric refrigeration relies on development of high-performance elastocaloric materials, the heart of the refrigeration device. Large elastocaloric effects have been observed in ferroelastic phase-transition materials [12] such as Cu-based shape memory alloys (SMAs) [10,13], NiTi-based SMAs [14–18] and NiMn-based Heusler-type magnetic SMAs [19,20]. Particularly, the prototype NiTi SMAs exhibit a giant elastocaloric effect [5,14,15]. Up to now, the highest elastocaloric effect with an adiabatic temperature change ΔT_{ad} up to 25 K is reported in NiTi wires, thin films, and foils [14–17], whereas bulk polycrystalline NiTi SMAs typically display a ΔT_{ad} below 15 K. For elastocaloric performance, the amount of heat transfer is proportional to the mass of the elastocaloric material and intimately related to the magnitude of the elastocaloric effect. However, it remains a great challenge to develop bulk polycrystalline materials with higher elastocaloric effects, which are essential for cost-effective large-scale cooling applications.

Here, by employing a novel design strategy, we achieved a colossal elastocaloric effect in a class of NiMn-based bulk polycrystalline alloys. The reversible ΔT_{ad} in these alloys reaches 31.5 K and the reversible isothermal entropy change is as large as 45 $\mathrm{J\,kg^{-1}\,K^{-1}}$. This reversible ΔT_{ad} far exceeds that directly measured in all elastocaloric, electrocaloric and barocaloric materials [21]. Furthermore, the working temperature of our alloys can be easily tuned for desired cooling and heat pumping applications. This study may inspire the discovery of giant caloric effects in a broad range of ferroelastic materials.

 © 2019 American Physical Society

The elastocaloric effect originates from the coupling between the lattice and the externally applied stress [10]. To achieve a reproducible large elastocaloric effect, the following strategy is employed. The basic concept mainly focuses on two points. First, the transformation entropy change ΔS_{tr} of the elastocaloric material must be large to provide great potential for achieving a large elastocaloric effect since ΔS_{tr} corresponds to the maximum attainable value for the stress-induced isothermal entropy change ΔS_{iso} [4,5]. Second, the mechanical properties of the elastocaloric material must be good enough to withstand a stress that is sufficiently high to fully induce the martensitic transformation, so that the potential for the large elastocaloric effect can be realized. For ferroelastic SMAs, the ΔS_{tr} for martensitic transformation can be expressed as $\Delta S_{tr} \approx \Delta S_{lat} + \Delta S_{mag} + \Delta S_{ele}$, where ΔS_{lat}, ΔS_{mag}, and ΔS_{ele} are the lattice (structural), magnetic, and electronic contributions to ΔS_{tr}, respectively, among which ΔS_{lat} plays a dominant role [23]. As is known, volume change is an important characteristic of first-order phase transitions [8]. Specifically, for martensitic transformation, the larger the unit cell volume change ($\Delta V/V_0$) across the transformation, the stronger the first-order transition, which leads to a larger ΔS_{lat} (and thus ΔS_{tr}) [24–26] [see Fig. 1(a) for example]. This is reasonable since the heat of formation of an intermetallic compound is proportional to the volume of formation of the compound from the component elements [24,27]. Therefore, we expect that a large elastocaloric effect to be achieved in ferroelastic alloys with simultaneous large $\Delta V/V_0$ and good mechanical properties.

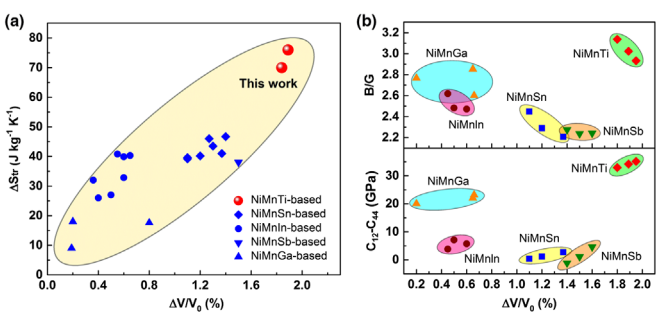

FIG. 1. Guide for the design of high-performance elastocaloric materials. (a) Correlation between transformation entropy change ΔS_{tr} and unit cell volume change $\Delta V/V_0$ across the transformation in NiMn-based Heusler alloys. The data are taken from the present work and literature (see Supplemental Material, Note 1 [28] for details). For "This work" the upper symbol is for $(Ni_{50}Mn_{31.5}Ti_{18.5})_{99.8}B_{0.2}$ and the lower one for $(Ni_{50}Mn_{32}Ti_{18})_{99.8}B_{0.2}$. All the data presented in this figure are taken from the alloys in which the martensitic transformation occurs above the Curie transition of austenite, namely, the magnetic contribution to ΔS_{tr} is negligible. (b) Ratio of bulk modulus B to shear modulus G, B/G and the Cauchy pressure C_{12}–C_{44}, obtained from *ab initio* calculations, plotted as a function of $\Delta V/V_0$ for NiMn-based Heusler alloys (see Supplemental Material, Note 1 [28] for detailed data).

To seek such ferroelastic alloys, NiMn-based Heusler-type SMAs are considered as potential candidates taking into account the large $\Delta V/V_0$ in the master alloy $Ni_{50}Mn_{50}$ [49]. In order to gain insight into mechanical properties of the NiMn-based Heusler-type SMAs, we performed *ab initio* calculations, using the exact muffin-tin orbitals (EMTO) method in combination with the coherent potentials approximation (CPA) (see Supplemental Material [28] for more details), to determine their elastic constants and moduli [Fig. 1(b)]. It is well acknowledged that the intrinsic brittle or ductile properties of metals can be reflected by the ratio of bulk modulus B to shear modulus G, B/G [50,51] and the Cauchy pressure C_{12}–C_{44} (C_{12} and C_{44} being elastic constants) [51,52]. The fact that the NiMnTi alloys exhibit the highest positive C_{12}–C_{44} and B/G [Fig. 1(b)] unambiguously indicates that it is most probable to achieve good mechanical properties in the NiMnTi system. Actually these NiMnTi alloys belong to the recently reported all-*d*-metal NiMnTi material family [53,54].

We thus prepared a series of $Ni_{50}Mn_{50-x}Ti_x$ (at. %) ($x = 12$–18.5) bulk polycrystalline alloys by arc melting and subsequent annealing at 1173 K for 48 h (see Supplemental Material [28] for details). Differential scanning calorimetry (DSC) measurements show that with increasing x, the martensitic transformation temperature decreases (Supplemental Material, Fig. 1 [28]). When x reaches 18 and 18.5, the transformation temperature is brought down to slightly below room temperature. Although the NiMnTi alloys show the least intrinsic brittleness in comparison with other NiMn-based alloys as indicated in Fig. 1(b), we further microalloyed the $Ni_{50}Mn_{50-x}Ti_x$ ($x = 18$ and 18.5) polycrystalline alloys with boron, since it is known that microalloying with boron enhances the grain boundary cohesion and improves the mechanical properties of NiMn-based Heusler-type SMAs [55,56]. It is found that microalloying with boron leads to decreasing transformation temperature (Supplemental Material, Fig. 2 [28]). For elastocaloric refrigeration the working temperature should be around room temperature, so we will focus on those alloys with transformation temperature slightly below room temperature: $(Ni_{50}Mn_{31.5}Ti_{18.5})_{99.8}B_{0.2}$ and $(Ni_{50}Mn_{32}Ti_{18})_{99.8}B_{0.2}$ (whose transformation temperatures can be found in the Supplemental Material, Fig. 2 [28]).

Our *in situ* synchrotron high-energy x-ray diffraction (HEXRD) experiments (as shown in detail later) reveal that these alloys do exhibit a large $\Delta V/V_0$: 1.89% for $(Ni_{50}Mn_{31.5}Ti_{18.5})_{99.8}B_{0.2}$ and 1.84% for $(Ni_{50}Mn_{32}Ti_{18})_{99.8}B_{0.2}$. Such $\Delta V/V_0$ values are much higher than those in other NiMn-based Heusler SMAs [Fig. 1(a)]. Thus, a large ΔS_{tr} is expected in these NiMnTiB alloys. It should be noted that ΔS_{ele} for this kind of NiMn-based Heusler alloy is very small [23], and ΔS_{mag} for the

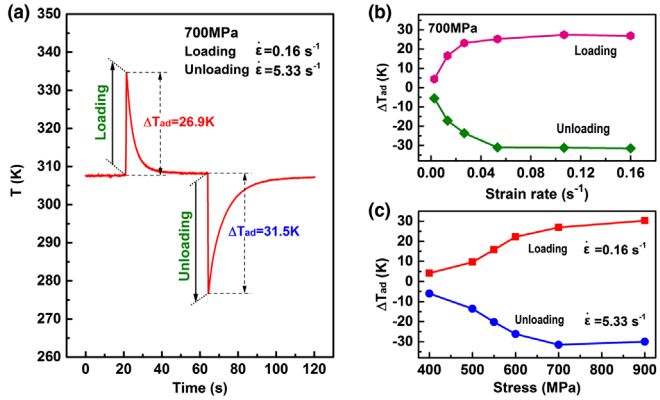

FIG. 2. Colossal adiabatic temperature change in $(Ni_{50}Mn_{31.5}Ti_{18.5})_{99.8}B_{0.2}$. (a) Temperature variation during loading, holding, and unloading, shown as a function of time. The maximum applied stress is 700 MPa, and the strain rate $\dot{\varepsilon}$ for loading and unloading is displayed in the figure. (b) Adiabatic temperature change as a function of strain rate $\dot{\varepsilon}$ (the same $\dot{\varepsilon}$ is applied for both loading and unloading), with the maximum applied stress of 700 MPa. (c) Adiabatic temperature change as a function of maximum applied stress, with loading and unloading rate $\dot{\varepsilon}$ of 0.16 and 5.33 s^{-1}, respectively.

present NiMnTiB alloys is negligible since their martensitic transformation occurs between paramagnetic austenite and paramagnetic martensite (Supplemental Material, Fig. 3 [28]); hence, the ΔS_{tr} for these alloys mainly comes from ΔS_{lat} which is directly linked to $\Delta V/V_0$. Indeed, our DSC measurements confirm that all the $Ni_{50}Mn_{50-x}Ti_x$ (at. %) ($x = 12$–18.5) alloys have a remarkably large ΔS_{tr}, in the range of 60–80 $J\,kg^{-1}\,K^{-1}$. Although the ΔS_{tr} decreases slightly with boron microalloying (Supplemental Material, Fig. 2 [28]), it still remains a much higher value [76 $J\,kg^{-1}\,K^{-1}$ for $(Ni_{50}Mn_{31.5}Ti_{18.5})_{99.8}B_{0.2}$ and 70 $J\,kg^{-1}\,K^{-1}$ for $(Ni_{50}Mn_{32}Ti_{18})_{99.8}B_{0.2}$] as compared with other NiMn-based Heusler alloys [5,56]. Therefore, a large elastocaloric effect can be expected in these alloys.

We investigated the elastocaloric effect of both $(Ni_{50}Mn_{31.5}Ti_{18.5})_{99.8}B_{0.2}$ and $(Ni_{50}Mn_{32}Ti_{18})_{99.8}B_{0.2}$, and found that the magnitude of their elastocaloric effect is similar and the only difference is the working temperature, owing to their different transformation temperatures. Hereafter we will focus on the results obtained from $(Ni_{50}Mn_{31.5}Ti_{18.5})_{99.8}B_{0.2}$, considering that its working temperature is around room temperature. The elastocaloric effect measurements were performed on cylindrical samples cut from the middle of the annealed button ingots; these samples show columnar grains displaying a strong texture with $\langle 001 \rangle$ of austenite parallel to the axial direction of the samples (see Supplemental Material [28] for details).

The adiabatic temperature change ΔT_{ad}, an important parameter for the elastocaloric effect, was examined by directly measuring the temperature variation of the sample during compressive loading and unloading, using a thermocouple (see Supplemental Material [28] for details). For such measurements [see Fig. 2(a)], the sample was first held at the testing temperature for a certain period [~20 s for Fig. 2(a)] and then loaded rapidly (within 1 s) to the maximum applied stress, followed by holding for t_1 [~40 s for Fig. 2(a)] to ensure the sample temperature recovers to the testing temperature, and subsequently unloaded rapidly (within 1 s) to 0 MPa followed by further holding for t_2 [~60 s for Fig. 2(a)]. The temperature variation for $(Ni_{50}Mn_{31.5}Ti_{18.5})_{99.8}B_{0.2}$ is shown as a function of time in Fig. 2(a). Strikingly, the sample temperature increases by 26.9 K during loading and decreases by as much as 31.5 K during unloading. Since the loading and unloading rates are high, these temperature changes are approximately taken as ΔT_{ad}. The sample temperature changes during loading and unloading are similar in magnitude (it should be mentioned that the loading and unloading rates are different), indicating that the ΔT_{ad} is reversible. Notably, this value of 31.5 K is a colossal reversible ΔT_{ad}, far exceeding that directly measured in all elastocaloric, electrocaloric, and barocaloric materials in any form (thin film, wire, bulk, etc.) (Table I) [21].

We systematically investigated the effect of strain rate $\dot{\varepsilon}$ and maximum applied stress σ_{max} on ΔT_{ad}. When σ_{max} is fixed at 700 MPa, ΔT_{ad} first increases rapidly for low $\dot{\varepsilon}$ and then tends to saturate above 0.05 s^{-1} [Fig. 2(b)]. This suggests that the adiabatic condition is approximately reached for $\dot{\varepsilon}$ above 0.05 s^{-1}. When the loading and unloading rates $\dot{\varepsilon}$ are fixed at 0.16 and 5.33 s^{-1}, respectively, ΔT_{ad} first increases with σ_{max} and then reaches saturation at $\sigma_{max} = 700$ MPa [Fig. 2(c)], indicating that 700 MPa is sufficient to induce the complete martensitic transformation under such $\dot{\varepsilon}$.

To examine the stress-induced isothermal entropy change ΔS_{iso}, which is the other important parameter for the elastocaloric effect, we measured the compressive stress-strain curves at different temperatures. ΔS_{iso} is computed based on the integration of the Maxwell relation [10], which gives $\Delta S_{iso} = \upsilon_0 \int_0^{\varepsilon} (\partial\sigma/\partial T)_{\varepsilon} d\varepsilon$, where υ_0 is the specific volume [1.42×10^{-4} $m^3\,kg^{-1}$ for the $(Ni_{50}Mn_{31.5}Ti_{18.5})_{99.8}B_{0.2}$ alloy studied here]. With the stress-strain curves displayed in Fig. 3(a), ΔS_{iso} is estimated numerically for different strain levels and shown as a function of temperature in Fig. 3(b). Remarkably, the ΔS_{iso} for 7% strain is as high as 45 $J\,kg^{-1}\,K^{-1}$. This ΔS_{iso} is reversible since the stress-strain loop indicates perfect superelasticity [the inset of Fig. 3(a)]. This reversible ΔS_{iso} is very large, as compared with other caloric materials (Table I). It is worth noting that our experimentally determined ΔT_{ad} and ΔS_{iso} can be well correlated with $\Delta T_{ad} \approx -(T\Delta S_{iso})/C_p$ where C_p is the specific heat capacity [4,5], which, for $(Ni_{50}Mn_{31.5}Ti_{18.5})_{99.8}B_{0.2}$, is around 470 $J\,kg^{-1}\,K^{-1}$ in the temperature range 280–320 K. In terms of the elastocaloric effect, the $(Ni_{50}Mn_{31.5}Ti_{18.5})_{99.8}B_{0.2}$ alloy (with a directly measured

TABLE I. Reversible adiabatic temperature change ΔT_{ad} and reversible isothermal entropy change ΔS_{iso} for typical caloric materials*.

Caloric material	T (K)	Reversible $\lvert\Delta T_{ad}\rvert$ (K)	Reversible $\lvert\Delta S_{iso}\rvert$ (J kg^{-1} K^{-1})	Field change	Ref.
Elastocaloric					
$(Ni_{50}Mn_{31.5}Ti_{18.5})_{99.8}B_{0.2}$ (bulk pc)	308	31.5	45	700 MPa	This work
$Ni_{48.9}Ti_{51.1}$ (wire)	330	25	35	900 MPa	[14]
$Ni_{50.4}Ti_{49.6}$ (film)	300	16	…	500 MPa	[16]
$Ni_{50.4}Ti_{49.6}$ (sc)	304	14	…	500 MPa	[57]
$Cu_{68.1}Zn_{15.8}Al_{16.1}$ (sc)	300	6	21	120 MPa	[10]
$Ni_{50}Fe_{19}Ga_{27}Co_4$ (sc)	348	10	…	300 MPa	[58]
$(Ni_{51.5}Mn_{33}In_{15.5})_{99.7}B_{0.3}$ (bulk pc)	303	6.6	…	550 MPa	[56]
Magnetocaloric					
Gd (bulk pc)	294	13	11	5 T	[59]
$Gd_5Si_2Ge_2$ (bulk pc)	280	15	19	5 T	[60]
$LaFe_{11.4}Mn_{0.4}Si_{1.3}H_{1.5}$ (bulk pc)	290	3	11	1.2 T	[61]
$MnFe_{0.95}P_{0.59}B_{0.08}Si_{0.33}$ (bulk pc)	280	2.6	10	1 T	[8]
$Ni_{49.8}Co_{1.2}Mn_{33.5}In_{15.5}$ (bulk pc)	235	…	14.6	5 T	[62]
$Ni_{45.7}Mn_{36.6}In_{13.5}Co_{4.2}$ (bulk pc)	282	3	…	2 T	[63]
Electrocaloric					
$PbZr_{0.46}Sn_{0.45}Ti_{0.1}O_3$ (bulk pc)	317	1.6	…	30 kV cm^{-1}	[64]
P(VDF-TrFE) (film)	340	12	…	1200 kV cm^{-1}	[4]
Barocaloric					
$Gd_5Si_2Ge_2$ (bulk pc)	270	1.1	11	0.20 GPa	[65]
$LaFe_{11.3}Co_{0.5}Si_{1.2}$ (bulk pc)	237	2.2	8.7	0.20 GPa	[9]

$\lvert\Delta T_{ad}\rvert$, reversible adiabatic temperature change obtained from direct measurements; $\lvert\Delta S_{iso}\rvert$, reversible isothermal entropy change derived from indirect measurements; T, testing temperature; pc, polycrystal; sc, single crystal; P(VDF-TrFE), poly(vinylidene fluoride–trifluoroethylene) 55/45 mol %. *Note: Only reliable data are included. Although a large $\lvert\Delta T_{ad}\rvert$ of 58 K was reported in a Ni-Ti foil (Ref. [66]), this value is not reliable because the $\lvert\Delta S_{iso}\rvert$ (~95 J kg^{-1} K^{-1}) derived via the relation $C_p\lvert\Delta T_{ad}\rvert \approx T\lvert\Delta S_{iso}\rvert$ (C_p, specific heat capacity) is significantly larger than the transformation entropy change ΔS_{tr} (~35 J kg^{-1} K^{-1}) experimentally determined therein (Ref. [66]), and therefore this value is not adopted.

reversible ΔT_{ad} of 31.5 K and a reversible ΔS_{iso} of 45 J kg^{-1} K^{-1}) well outperforms the prototype NiTi elastocaloric materials (typically with a maximum ΔT_{ad} of ~25 K and ΔS_{iso} of ~35 J kg^{-1} K^{-1}) (Table I). It is worth mentioning that the ΔS_{iso} we achieved is lower than the ΔS_{tr} determined from DSC measurements under zero stress. Two possible reasons are (i) the transformation strain is lower if the transformation occurs under a higher stress [Fig. 3(a)], which, according to the Clausius-Clapeyron relation [10], leads to the decrease of transformation entropy change with increasing stress and (ii) the entropy change associated with the transformation from austenite to multivariant martensite under zero stress is different from that associated with the stress-induced transformation from austenite to single-variant martensite [10].

To better understand the colossal elastocaloric effect and its underlying mechanism, we performed *in situ* synchrotron HEXRD experiments to trace the structural evolution during loading and unloading (Fig. 4 and Supplemental Material, Figs. 4 and 5 [28]). The experiments were performed at 295 K and a monochromatic x-ray beam with a wavelength of 0.1173 Å was used. The stress was applied with a loading frame controlled by displacement. As indicated from Fig. 4(a), the sample exhibits a Heusler austenite structure (space group $Fm\bar{3}m$, No. 225) with lattice parameter $a_0 = 5.945$ Å before loading. Upon loading, it transforms into an orthorhombic (space group $Pmma$, No. 51) martensite with lattice parameters $a_M = 8.553$, $b_M = 5.505$, and $c_M = 4.378$ Å (Supplemental Material, Fig. 4 [28]). Notably, the stress-induced martensitic transformation is fully accomplished when the stress reaches above 413 MPa [Fig. 4(a) and Supplemental Material, Fig. 5 [28]]. During unloading, the stress-induced martensite fully transforms back to austenite (Fig. 4). As seen from Fig. 4(b), the 2D HEXRD patterns collected before loading and after unloading are almost identical, indicating that the stress-induced transformation is fully reversible. The completeness and reversibility of the stress-induced transformation are important for the achievement of the colossal reversible elastocaloric effect. Based on the lattice parameters of austenite and martensite, the unit cell volume change across the transformation $\Delta V/V_0$ is determined to be 1.89% for $(Ni_{50}Mn_{31.5}Ti_{18.5})_{99.8}B_{0.2}$. This large $\Delta V/V_0$ accounts for the large ΔS_{tr}, which is a prerequisite for the colossal elastocaloric effect. It is worth noting that the stress required for inducing complete transformation is different

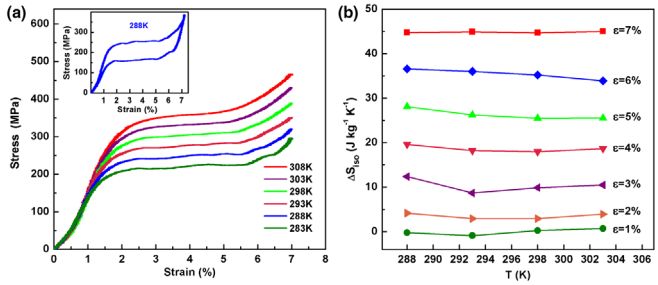

FIG. 3. Stress-induced isothermal entropy change in $(Ni_{50}Mn_{31.5}Ti_{18.5})_{99.8}B_{0.2}$. (a) Compressive stress-strain curves measured with a low strain rate of 1.3×10^{-4} s^{-1} at different temperatures. For clarity, only the curves recorded during loading are displayed. The inset shows a full stress-strain loop measured at 288 K, as an example. (b) Isothermal entropy change for different strain levels, shown as a function of temperature. The data are derived from the stress-strain curves displayed in (a).

in the *in situ* HEXRD experiment (Fig. 4) and elastocaloric effect measurements [Figs. 2(c) and 3(a)], which is attributed to the different strain rates and testing temperatures (a detailed explanation is presented in the Supplemental Material, Note 2 [28]).

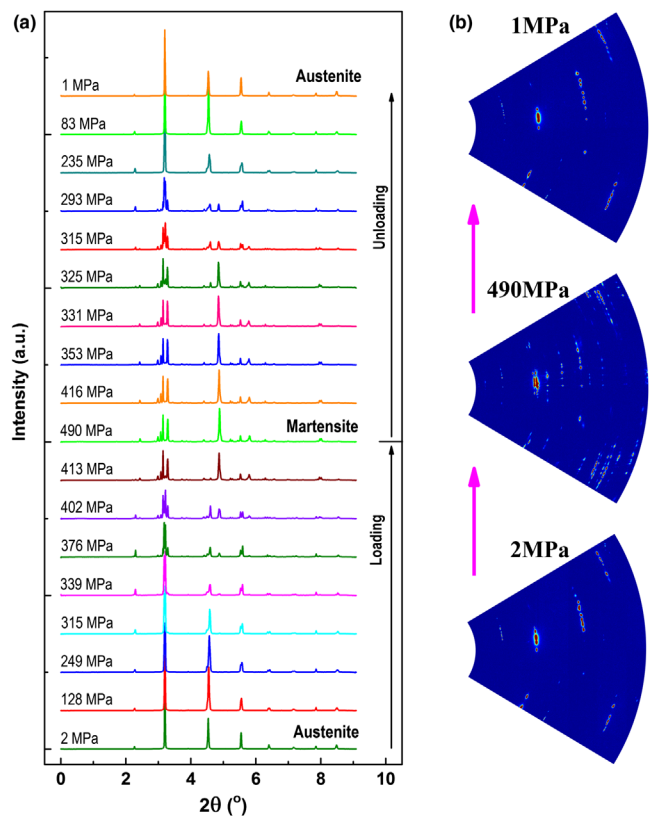

FIG. 4. Crystal structure evolution during stress-induced transformation in $(Ni_{50}Mn_{31.5}Ti_{18.5})_{99.8}B_{0.2}$. (a) 1D HEXRD patterns at different stress levels during loading and unloading at 295 K. (b) Representative zone of the 2D HEXRD patterns collected before loading (2 MPa), at the maximum stress (490 MPa), and after unloading (1 MPa) at 295 K.

In conclusion, we have achieved a colossal elastocaloric effect in a class of bulk polycrystalline NiMnTiB alloys designed with the criterion of having simultaneous large volume change across phase transition and good mechanical properties. The reversible ΔT_{ad} reaches a strikingly high value of 31.5 K, which represents the largest reversible ΔT_{ad} directly measured in all elastocaloric, electrocaloric, and barocaloric materials (Table I) [21]. The reversible ΔS_{iso} is as large as 45 $J\,kg^{-1}\,K^{-1}$. Furthermore, the working temperature of the present NiMnTiB alloys can be easily tuned for refrigeration and heat pump applications at different temperatures. We anticipate that the achievement of such a colossal elastocaloric effect in bulk polycrystalline materials that are inexpensive to fabricate and can be easily scaled up will push a significant step forward towards large-scale applications of high-efficiency and environment-friendly elastocaloric refrigeration. Moreover, the present design strategy opens a new avenue for discovering giant caloric effects in ferroelastic materials.

Professor Levente Vitos and Dr. Fuyang Tian are acknowledged for discussions on the EMTO-CPA method and *ab initio* calculation results. We are grateful to Professor David Long Price and Professor Marie-Louise Saboungi for critically reading the manuscript. This work was supported by the National Natural Science Foundation of China (No. 51822102, No. 51731005, and No. 51527801) and the Fundamental Research Funds for the Central Universities (No. FRF-TP-18-008C1). Use of the Advanced Photon Source was supported by the U.S. Department of Energy, Office of Science, Office of Basic Energy Science, under Contract No. DE-AC02-06CH11357. A. P. and L. M. acknowledge the support from the Spanish Ministry of Economy and Competitiveness, Project No. MAT2016-75823-R.

*Corresponding author.
dycong@ustb.edu.cn

[1] Energy savings potential and RD&D opportunities for non-vapor-compression HVAC technologies, Report of the U.S. Department of Energy, 2014, https://energy.gov/eere/buildings/downloads/non-vapor-compression-hvac-technologies-report.
[2] O. Tegus, E. Brück, K. H. J. Buschow, and F. R. de Boer, Nature (London) **415**, 150 (2002).
[3] D. Matsunami, A. Fujita, K. Takenaka, and M. Kano, Nat. Mater. **14**, 73 (2015).
[4] X. Moya, S. Kar-Narayan, and N. D. Mathur, Nat. Mater. **13**, 439 (2014).
[5] L. Mañosa and A. Planes, Adv. Mater. **29**, 1603607 (2017).
[6] B. Neese, B. Chu, S. Lu, Y. Wang, E. Furman, and Q. M. Zhang, Science **321**, 821 (2008).
[7] J. Liu, T. Gottschall, K. P. Skokov, J. D. Moore, and O. Gutfleisch, Nat. Mater. **11**, 620 (2012).
[8] F. Guillou, G. Porcari, H. Yibole, N. van Dijk, and E. Brück, Adv. Mater. **26**, 2671 (2014).

[9] P. Lloveras, E. Stern-Taulats, M. Barrio, J. L. Tamarit, S. Crossley, W. Li, V. Pomjakushin, A. Planes, L. Mañosa, N. D. Mathur, and X. Moya, Nat. Commun. **6**, 8801 (2015).

[10] E. Bonnot, R. Romero, L. Mañosa, E. Vives, and A. Planes, Phys. Rev. Lett. **100**, 125901 (2008).

[11] J. Tušek, K. Engelbrecht, D. Eriksen, S. Dall'olio, J. Tušek, and N. Pryds, Nat. Energy **1**, 16134 (2016).

[12] E. K. H. Salje, Annu. Rev. Mater. Res. **42**, 265 (2012).

[13] S. Xu, H. Y. Huang, J. Xie, S. Takekawa, X. Xu, T. Omori, and R. Kainuma, APL Mater. **4**, 106106 (2016).

[14] J. Tušek, K. Engelbrecht, R. Millán-Solsona, L. Mañosa, E. Vives, L. P. Mikkelsen, and N. Pryds, Adv. Energy Mater. **5**, 1500361 (2015).

[15] J. Cui, Y. Wu, J. Muehlbauer, Y. Hwang, R. Radermacher, S. Fackler, M. Wuttig, and I. Takeuchi, Appl. Phys. Lett. **101**, 073904 (2012).

[16] H. Ossmer, F. Lambrecht, M. Gültig, C. Chluba, E. Quandt, and M. Kohl, Acta Mater. **81**, 9 (2014).

[17] C. Bechtold, C. Chluba, R. Lima de Miranda, and E. Quandt, Appl. Phys. Lett. **101**, 091903 (2012).

[18] X. Liang, F. Xiao, M. Jin, X. Jin, T. Fukuda, and T. Kakeshita, Scr. Mater. **134**, 42 (2017).

[19] P. Álvarez-Alonso, C. O. Aguilar-Ortiz, E. Villa, A. Nespoli, H. Flores-Zúñiga, and V. A. Chernenko, Scr. Mater. **128**, 36 (2017).

[20] Y. J. Huang, Q. D. Hu, N. M. Bruno, J. H. Chen, I. Karaman, J. H. Ross, and J. G. Li, Scr. Mater. **105**, 42 (2015).

[21] Actually this reversible ΔT_{ad} is also much higher than that directly measured in most magnetocaloric materials, although a ΔT_{ad} of 60 K was obtained under an extremely high magnetic field of 55 T, which is unlikely to be accessible for practical applications, in Gd in Ref. [22].

[22] T. Kihara, Y. Kohama, Y. Hashimoto, S. Katsumoto, and M. Tokunaga, Rev. Sci. Instrum. **84**, 074901 (2013).

[23] V. Recarte, J. I. Pérez-Landazábal, V. Sánchez-Alarcos, V. Zablotskii, E. Cesari, and S. Kustov, Acta Mater. **60**, 3168 (2012).

[24] K. A. Gschneidner, Y. Mudryk, and V. K. Pecharsky, Scr. Mater. **67**, 572 (2012).

[25] T. Samanta, D. L. Lepkowski, A. U. Saleheen, A. Shankar, J. Prestigiacomo, I. Dubenko, A. Quetz, I. W. H. Oswald, G. T. McCandless, J. Y. Chan, P. W. Adams, D. P. Young, N. Ali, and S. Stadler, Phys. Rev. B **91**, 020401(R) (2015).

[26] P. Shamba, J. L. Wang, J. C. Debnath, R. Zeng, F. Hong, Z. X. Cheng, A. J. Studer, S. J. Kennedy, and S. X. Dou, J. Appl. Phys. **113**, 17A941 (2013).

[27] O. Kubaschewski, C. B. Alcock, and P. J. Spenser, *Materials Thermochemistry*, 6th ed. (Pergamon Press, Oxford, UK, 1993).

[28] See Supplemental Material http://link.aps.org/supplemental/10.1103/PhysRevLett.122.255703 for experimental details and supplemental figures and notes, which includes Refs. [29–48].

[29] S. Fabbrici, J. Kamarad, Z. Arnold, F. Casoli, A. Paoluzi, F. Bolzoni, R. Cabassi, M. Solzi, G. Porcari, C. Pernechele, and F. Albertini, Acta Mater. **59**, 412 (2011).

[30] S. Y. Yu, Z. X. Cao, L. Ma, G. D. Liu, J. L. Chen, G. H. Wu, B. Zhang, and X. X. Zhang, Appl. Phys. Lett. **91**, 102507 (2007).

[31] F. Albertini, S. Fabbrici, A. Paoluzi, J. Kamarad, Z. Arnold, L. Righi, M. Solzi, G. Porcari, C. Pernechele, D. Serrate, and P. Algarabel, Mater. Sci. Forum **684**, 151 (2011).

[32] E. Stern-Taulats, A. Planes, P. Lloveras, M. Barrio, J. L. Tamarit, S. Pramanick, S. Majumdar, S. Yüce, B. Emre, C. Frontera, and L. Mañosa, Acta Mater. **96**, 324 (2015).

[33] M. K. Chattopadhyay, V. K. Sharma, A. Chouhan, P. Arora, and S. B. Roy, Phys. Rev. B **84**, 064417 (2011).

[34] L. Mañosa, D. González-Alonso, A. Planes, E. Bonnot, M. Barrio, J. L. Tamarit, S. Aksoy, and M. Acet, Nat. Mater. **9**, 478 (2010).

[35] L. Mañosa, X. Moya, A. Planes, O. Gutfleisch, J. Lyubina, M. Barrio, J. L. Tamarit, S. Aksoy, T. Krenke, and M. Acet, Appl. Phys. Lett. **92**, 012515 (2008).

[36] C. O. Aguilar-Ortiz, D. Soto-Parra, P. Alvarez-Alonso, P. Lazpita, D. Salazar, P. O. Castillo-Villa, H. Flores-Zúñiga, and V. A. Chernenko, Acta Mater. **107**, 9 (2016).

[37] T. Krenke, M. Acet, E. F. Wassermann, X. Moya, L. Mañosa, and A. Planes, Phys. Rev. B **72**, 014412 (2005).

[38] V. Recarte, M. Zbiri, M. Jiménez-Ruiz, V. Sánchez-Alarcos, and J. I. Pérez-Landazábal, J. Phys. Condens. Matter **28**, 205402 (2016).

[39] S. Aksoy, M. Acet, E. F. Wassermann, T. Krenke, X. Moya, L. Manosa, A. Planes, and P. P. Deen, Philos. Mag. **89**, 2093 (2009).

[40] Y. Tanaka, Y. Himuro, R. Kainuma, Y. Sutou, T. Omori, and K. Ishida, Science **327**, 1488 (2010).

[41] L. Vitos, *Computational Quantum Mechanics for Materials Engineers: The EMTO Method and Applications* (Springer Science & Business Media, London, UK, 2007).

[42] L. Vitos, P. A. Korzhavyi, and B. Johansson, Nat. Mater. **2**, 25 (2003).

[43] L. Vitos, I. A. Abrikosov, and B. Johansson, Phys. Rev. Lett. **87**, 156401 (2001).

[44] P. Cao, X. Ni, F. Tian, L. K. Varga, and L. Vitos, J. Phys. Condens. Matter **27**, 075401 (2015).

[45] C. M. Li, Q. M. Hu, R. Yang, B. Johansson, and L. Vitos, Phys. Rev. B **91**, 174112 (2015).

[46] V. V. Sokolovskiy, P. Entel, V. D. Buchelnikov, and M. E. Gruner, Phys. Rev. B **91**, 220409(R) (2015).

[47] S. Singh, S. W. D'Souza, J. Nayak, L. Caron, E. Suard, S. Chadov, and C. Felser, Phys. Rev. B **93**, 134102 (2016).

[48] J. P. Perdew, K. Burke, and M. Ernzerhof, Phys. Rev. Lett. **77**, 3865 (1996).

[49] P. L. Potapov, N. A. Polyakova, V. A. Udovenko, and E. L. Svistunova, Z. Metallkd. **87**, 33 (1996).

[50] S. F. Pugh, Philos. Mag. **45**, 823 (1954).

[51] D. G. Pettifor and A. H. Cottrell, *Electron Theory in Alloy Design* (The Institute of Materials, London, UK, 1992).

[52] D. G. Pettifor, Mater. Sci. Technol. Lond. **8**, 345 (1992).

[53] Z. Y. Wei, E. K. Liu, J. H. Chen, Y. Li, G. D. Liu, H. Z. Luo, X. K. Xi, H. W. Zhang, W. H. Wang, and G. H. Wu, Appl. Phys. Lett. **107**, 022406 (2015).

[54] Z. Y. Wei, E. K. Liu, Y. Li, X. L. Han, Z. W. Du, H. Z. Luo, G. D. Liu, X. K. Xi, H. W. Zhang, W. H. Wang, and G. H. Wu, Appl. Phys. Lett. **109**, 071904 (2016).

[55] Y. Aydogdu, A. S. Turabi, M. Kok, A. Aydogdu, H. Tobe, and H. E. Karaca, Appl. Phys. A **117**, 2073 (2014).

[56] Z. Yang, D. Y. Cong, X. M. Sun, Z. H. Nie, and Y. D. Wang, Acta Mater. **127**, 33 (2017).

[57] G. J. Pataky, E. Ertekin, and H. Sehitoglu, Acta Mater. **96**, 420 (2015).
[58] F. Xiao, M. Jin, J. Liu, and X. Jin, Acta Mater. **96**, 292 (2015).
[59] S. Y. Dan'Kov, A. M. Tishin, V. K. Pecharsky, and K. A. Gschneidner, Phys. Rev. B **57**, 3478 (1998).
[60] V. K. Pecharsky and K. A. Gschneidner, Jr., Phys. Rev. Lett. **78**, 4494 (1997).
[61] K. Morrison, K. G. Sandeman, L. F. Cohen, C. P. Sasso, V. Basso, A. Barcza, M. Katter, J. D. Moore, K. P. Skokov, and O. Gutfleisch, Int. J. Refrig. **35**, 1528 (2012).
[62] L. Huang, D. Y. Cong, L. Ma, Z. H. Nie, Z. L. Wang, H. L. Suo, Y. Ren, and Y. D. Wang, Appl. Phys. Lett. **108**, 032405 (2016).
[63] T. Gottschall, K. P. Skokov, B. Frincu, and O. Gutfleisch, Appl. Phys. Lett. **106**, 021901 (2015).
[64] P. D. Thacher, J. Appl. Phys. **39**, 1996 (1968).
[65] S. Yuce, M. Barrio, B. Emre, E. Stern-Taulats, A. Planes, J. L. Tamarit, Y. Mudryk, K. A. Gschneidner, Jr., V. K. Pecharsky, and L. Mañosa, Appl. Phys. Lett. **101**, 071906 (2012).
[66] E. A. Pieczyska, H. Tobushi, and K. Kulasinski, Smart Mater. Struct. **22**, 035007 (2013).